J Nanopart Res (2024) 26:183
https://doi.org/10.1007/s11051-024-06095-z

RESEARCH

Hydrogen Evolution Reaction Activity of Electrochemically Exfoliated Borophene

Suleyman Can · Duygu Kuru · Cihan Kuru

Received: 4 June 2024 / Accepted: 29 July 2024 / Published online: 6 August 2024

Abstract Borophene has been theoretically shown as an active catalyst for hydrogen evolution reaction (HER). However, there are a few experimental studies assessing the HER activity of borophene. Herein, we study for the first time HER activity of electrochemically exfoliated borophene in acidic medium. Borophene sheets obtained by anodic exfoliation of crystalline boron particles in Na_2SO_4 have β-rhombohedral crystal structure with an oxidized surface. Borophene exhibits notably higher catalytic activity compared to bulk boron with an overpotential of 480 mV at 10 mA cm^{-2} and a Tafel slope of 163 mV dec^{-1}. The superior activity of borophene is attributed to enhanced HER kinetics as well as increased electrochemical surface area. Our study provides encouraging results for the use of borophene in catalysis applications.

Keywords Borophene · Catalyst · Electrochemical exfoliation · Hydrogen revolution reaction · Nanostructures

S. Can · C. Kuru (✉)
Department of Metallurgical and Materials Engineering, Bilecik Seyh Edebali University, Bilecik 11100, Turkey
e-mail: cihan.kuru@bilecik.edu.tr

D. Kuru
Department of Chemical Engineering, Bilecik Seyh Edebali University, Bilecik 11100, Turkey

Introduction

Energy demand has been relentlessly growing as the world population increases. Fossil fuels have been the main energy source in the last two centuries to meet world's energy demand. However, fossil fuels are nonrenewable, cause air pollution and emit significant amount of CO_2 into the atmosphere, leading to greenhouse effect [1–3]. Since the beginning of industrial revolution, the average temperature of earth has risen by 0.8 °C [4]. In 2016, Paris agreement was signed in an effort to mitigate the effects of global warming. The treaty aims to limit the temperature increase to 1.5 °C, which requires becoming climate neutral by 2050 [5]. To achieve this goal, fossil fuel consumption must be reduced to a great extent. Alternately, green hydrogen can be used to power up vehicles, to heat up residential buildings and to provide energy for industrial use. Hydrogen is a promising energy carrier because it has high gravimetric energy density [6], produces no harmful by-products and can be converted to electricity via fuel cells with high efficiency. In addition, hydrogen can be regarded as a way of energy storage for unused renewable energy, which could potentially minimize energy wastage.

Current hydrogen production primarily relies on steam reduction of hydrocarbons [7], which does not overcome the above-mentioned problems. On the other hand, electrochemical water splitting

where the energy input is provided by renewable energy sources is a sustainable method for green hydrogen production. However, low efficiency and high cost of this method hinders its adoption in transition to hydrogen economy [8]. A key element to the electrochemical water splitting is catalysts that minimize energy losses at electrode/electrolyte interface, leading to more efficient electrolysers [9–11]. In that sense, high efficiency, low cost and durable electrocatalysts are highly desired.

2D electrocatalysts have great potential in water splitting reactions owing to their large exposed surface area, low charge transfer resistance and tunable chemical properties [12–15]. 2D materials comprising transition metal dichalcogenides (TMDs) and MXenes have been extensively studied in hydrogen evolution reaction (HER) [16–20]. Recently, a new class of 2D materials has emerged as elemental 2D materials, which include phosphorene, bismuthane, silicene, tellurene, arsenene, antimonene, stanene and borophene [21–23]. Among those, borophene has been drawing great interest because of the diversified and complex bonding structure that leads to polymorphism and strong anisotropy with intriguing mechanical, electronic and chemical properties [24–27]. Borophene has been predicted as an active catalyst for HER with a Gibbs free energy of hydrogen adsorption (ΔG_H) close to zero [28, 29]. In addition, borophene exhibits metallic conductivity [30], which is highly desirable for electrocatalysis. Although a few theoretical studies have been published on the catalytic activity of borophene [31–33], there have been only two attempts to experimentally demonstrate borophene in HER. Tai et al. used chemical vapor deposition (CVD) to synthesize borophene sheets on carbon cloth, which showed a promising HER performance with an overpotential of 142 mV at 10 mA cm^{-2} and a Tafel slope of 69 mV dec^{-1} [34]. In the other study, borophene sheets produced by surfactant-assisted liquid phase exfoliation method exhibited a 645 mV overpotential and 173 mV dec^{-1} Tafel slope [35].

Initial effort to produce borophene was primarily based on bottom-up approaches which result in borophene films on various metal substrates [36–38]. Later on, freestanding borophene could be prepared by sono-chemical methods [39–42]. In a recent study, we successfully prepared freestanding borophene sheets by anodic exfoliation of boron powder [43]. Motivated by our achievement and lack of experimental data on the catalytic activity of borophene in HER, here we study the HER performance of the electrochemically exfoliated borophene sheets. The structural and chemical properties of the borophene sheets were investigated by various characterization methods. The HER performance of the borophene sheets was determined in acidic conditions by electrochemical measurements, in which borophene sheets showed notably higher performance compared to bulk boron particles.

Experimental

Electrochemical exfoliation

The electrochemical exfoliation procedure of boron was described in detail in our previous study [43]. Briefly, 375 mg of crystalline boron powder, 125 mg of multiwalled carbon nanotubes (MWCNTs) and 50 mg of polymethyl methacrylate (PMMA) binder dissolved in acetone were mixed together in isopropyl alcohol (IPA) using a bath sonicator and dried overnight at 80 °C in an oven. Subsequently, the dried powder was pressed into a circular pellet at 500 bar using a manual hydraulic press. The pellet electrode was anodically exfoliated in a 1:1 (v/v) mixture of 1 molar sodium sulfate (Na_2SO_4) and glycerin at 30 V. The MWCNTs provided the necessary electrical conductivity to the electrode for the electrochemical exfoliation and subsequently removed by a two-step process: First, majority of the MWCNTs were removed by collecting borophene sheets with a separation funnel from a toluene/water system where borophene sheets were dispersed in the water section while the MWCNTs accumulated at the interface region upon sonication. Second, residual MWCNTs were filtrated through a cellulose membrane with a pore size of 8 µm. Finally, the purified borophene sheets were collected on a filtration membrane and redispersed in H_2O/IPA mixture (1:1 v/v) and centrifuged at 4500 rpm for 20 min. Borophene powder was obtained by freeze drying at a temperature of -37 °C and a pressure of 0.18 bar for 24 h.

Characterization

Fourier transform infrared (FTIR) spectroscopy measurements were performed in Perkin Elmer Spectrum 100 spectrometer using KBr method. Raman spectrum was obtained on a WITec alpha 300R spectrophotometer with a laser wavelength of 532 nm and power of 5 mW. X-ray diffraction (XRD) data was collected by Rigaku D-Max with Cu-Kα X-ray source (1.54 Å). X-ray photoelectron spectroscopy (XPS) measurements were conducted on SPECS FlexMod spectrometer using Al-Kα radiation source (1486.71 eV). High resolution transmission electron microscopy (HRTEM) and energy dispersive X-ray spectroscopy (EDX) mapping analysis were carried out with FEI TALOS F200S TEM. Atomic force microscopy (AFM) images were taken with Hitachi 5100N in tapping mode. Scanning electron microscopy (SEM) image and EDX spectrum were obtained with FEI Quanta FEG 450 scanning electron microscope.

Electrochemical Measurements

Four mg of borophene powder, 4 mg of carbon black (superP) and 50 µl of nafion solution (5%) were dispersed in 0.5 ml of H_2O/IPA mixture by sonication for 30 min. 50 µl of the dispersion was drop casted on a graphite rod electrode whose sidewalls are isolated by a heat shrink tube. Prior to catalyst loading, the surface of the graphite electrode was polished with a fine emery paper and cleaned with IPA. Electrochemical measurements were performed with Gamry Interface 1000 potentiostat in a three-electrode set-up. Graphite rod, Pt wire and saturated calomel electrode (SCE) were used as the working, counter and reference electrodes, respectively. The electrolyte was 0.5 M H_2SO_4, which was deaerated with N_2 gas and stirred at 500 rpm during the measurements. The reference electrode potential has been converted to reversible hydrogen electrode (RHE) potential using the relation: $E(RHE) = E(SCE) + 0.241V$. Linear sweep voltammetry (LSV) measurements were conducted between 0 and -0.7 V vs. RHE with a scan rate of 5 mV s^{-1}. The LSV data have been compensated (100%) for ohmic drop after measuring solution resistance using Gamry software. Typical solution resistance values ranged from 4 to 6 ohms. Electrochemical impedance spectroscopy (EIS) data were obtained at an overpotential of 480 mV between 1 Hz and 1 MHz. The amplitude of the DC bias was 10 mV. Cyclic voltammetry (CV) measurements were taken in the potential range of 0.1–0.3 V vs. RHE at different scan rates (20, 40, 60, 80 and 100 mV s^{-1}). Double layer capacitance (C_{dl}) was calculated from the half slope of the Δj vs. scan rate plot, where Δj is the current density difference of the forward and reverse CV scans.

Results and discussion

The electrochemical exfoliation of crystalline boron was conducted in a two-electrode set-up at + 30 V (Fig. 1a). A boron/MWCNTs composite electrode was used for the electrochemical exfoliation, where the MWCNTs provided the necessary electrical conductivity. The MWCNTs were removed after the exfoliation process. The final dispersion exhibits the typical brown color of borophene, which indicates the successful separation of the MWCNTs (Fig. 1b). AFM measurements were carried out to evaluate the thickness and lateral size of the produced borophene sheets.

The AFM image of the borophene sheets coated on a SiO_2/Si substrate and the height profiles of the marked lines are shown in Fig. 1c and d. The thickness of the sheets ranges from 2 to 25 nm with 35% of them being less than 5 nm thick. The average thickness and lateral size of the sheets were calculated as 8.7 and 104 nm, respectively (Fig. 1 e and f).

TEM measurements were conducted to evaluate the structure of the borophene sheets. Low resolution TEM image of a thin borophene sheet shown in Fig. 2a proves the successful exfoliation of the boron particles. Lattice fringes are clearly visible in high resolution TEM image (Fig. 2b and c), suggesting the high crystallinity of the borophene sheet. The calculated interplanar distance is 4.6 Å, which corresponds to (021) plane of β-rhombohedral boron [44]. EDX analysis indicates the oxidized surface of the borophene sheet (Fig. 2d-f).

Raman spectroscopy measurements were performed to investigate the structural properties of

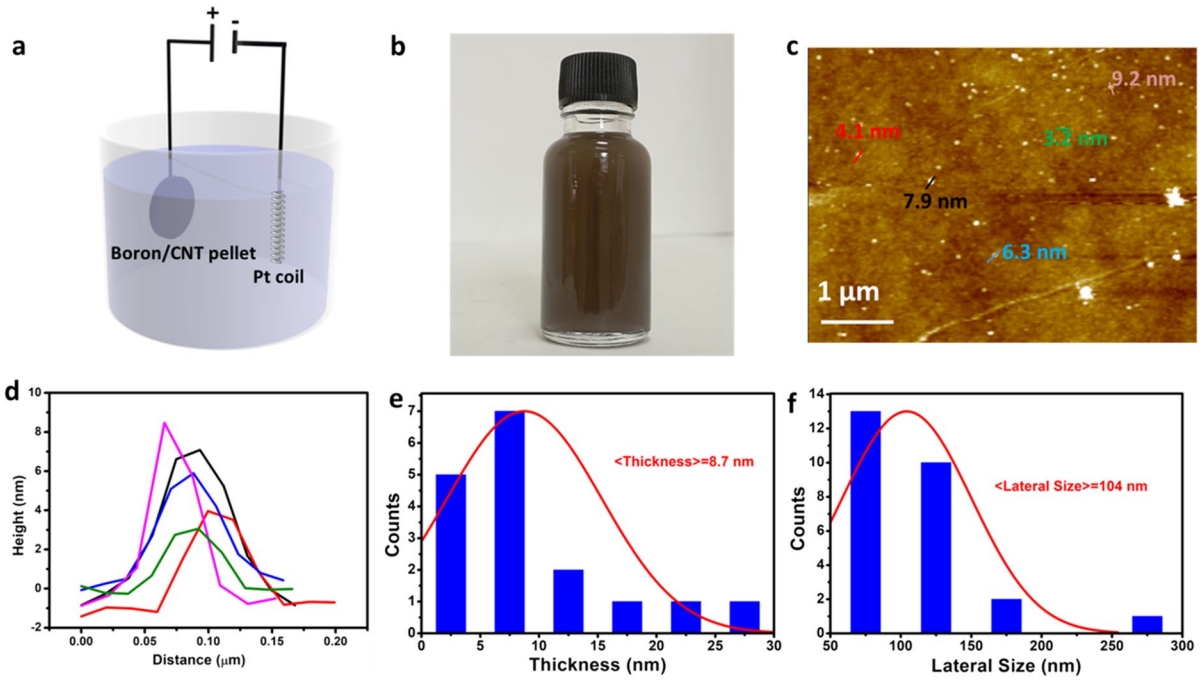

Fig. 1 (**a**) Schematic picture of the set-up used for the electrochemical exfoliation of boron. (**b**) Optical image of the final borophene dispersion. (**c**) AFM image of the borophene sheets coated on SiO_2/Si substrate. (**d**) Height profiles of the colored lines marked on the AFM image. (**e**) Thickness and (**f**) lateral size histograms of the borophene sheets

borophene. Raman spectra of bulk boron and the borophene sheets drop casted on a Cu foil are depicted in Fig. 3a, in which six major peaks appear at 298, 435, 641, 738, 781 and 1084 cm^{-1}, which correspond to β boron [45]. Among those, the peaks at 435 and 738 could be matched with $B_g^1(Y)$ and A_g^3 modes of χ_3 phase whereas the peaks at 298 and 1084 cm^{-1} could be either related to $A_u(Y)$ and A_g^2 modes of χ_3 or B_{1u}^2 and B_{1g}^1 modes of β_{12} phase as both phases exhibit vibration modes in the same vicinity [46]. As a reference, the theoretically calculated and experimentally observed frequency values of the $B_g^1(Y)$, A_g^3,$A_u(Y)$, A_g^2, B_{1u}^2 and B_{1g}^1 modes are 460/445, 769/745, 306/291, 1091/1077, 292/296 and 1026/1060, respectively [46]. In comparison, vapor phase grown borophene exhibits Raman features of both β_{12} and χ_3 phases and its Raman spectrum differs from bulk boron [47, 48]. Similar Raman modes detected for both bulk boron and exfoliated borophene sheets may be due to relatively large thickness of the sheets. FTIR and XPS measurements were performed to analyze the chemistry of the surface of the borophene sheets. FTIR spectrum of the borophene powder obtained after the electrochemical exfoliation is shown in Fig. 3b. The stretching modes corresponding to B-O-B (1053 cm^{-1}) [49], B-O (1224 cm^{-1}) [49], C-H (1361, 1394, 2823 and 2883 cm^{-1}) [50] and C = C (1629 cm^{-1}) [51] bonds could be identified. The C-H and C = C bonds are most likely originated from the PMMA residue. Figure 3c exhibits the B 1 s XPS spectrum of borophene sheets drop casted on a Si substrate. B 1 s spectrum of borophene was deconvoluted into three different peaks centered at 187.4, 188.6 and 192.0 eV which are associated to boron-boron (B-B), boron-suboxide (B-O) and boron trioxide (B_2O_3) bonds, respectively. Similar peaks have been observed by others [42, 44, 52]. The B-O bond is most likely resulted from the oxidation of borophene surface in contact with air whereas the B_2O_3 bond could be related to the electrochemical reactions taking place on the surface of the boron particles during the exfoliation process. The

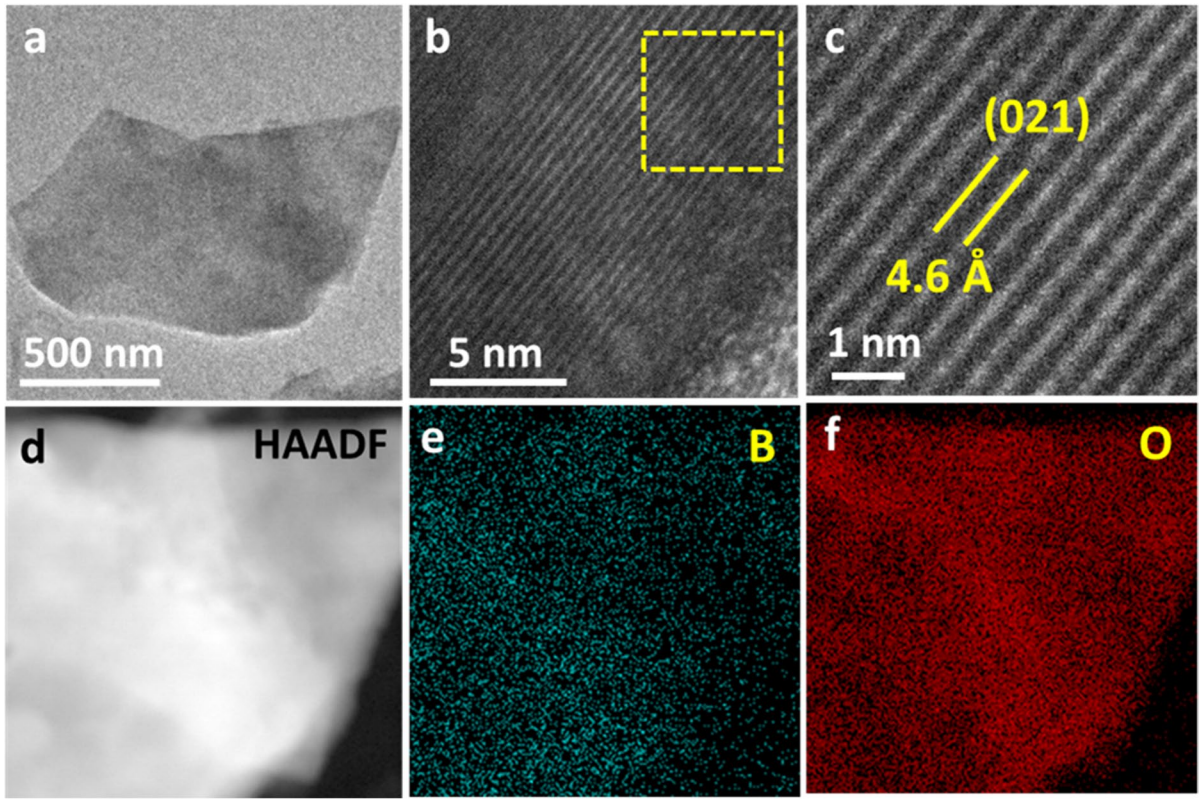

Fig. 2 (**a**) Low and (**b**) high resolution TEM images of a borophene sheet. (**c**) Close up image of the region marked by yellow dashed square. (**d**) HAADF image of the borophene sheet. EDX mapping images of (**e**) B and (**f**) O elements

percentage of the B-B, B-O and B_2O_3 bonds were estimated to be 56%, 36% and 8% through peak area integration. The amount of oxidation is comparable to borophene produced by sono-chemical and ball milling methods [42, 44] and lower than vapor phase grown borophene [38]. The crystal structure of borophene was determined by XRD measurements. The XRD patterns of crystalline boron powder and the borophene sheets collected on a Nylon filter membrane were compared in Fig. 3d. The XRD pattern of the crystalline boron powder matches well with β-rhombohedral crystal structure consisting of 105 B atom in the unit cell (B_{105}-PDF# 01–072-1705). On the other hand, borophene exhibits a similar XRD pattern with crystalline boron, suggesting that the crystal structure of boron was preserved after the exfoliation. Overall, the intensity of the XRD peaks of borophene is low compared to bulk boron and some peaks disappeared after the exfoliation, which could be attributed to thinning of the boron particles. Two new peaks were detected for borophene at 38.18° and 77.37°, which correspond to B_2O (PDF# 00–041-0624). The B_2O peaks arise from the boron-suboxide phase formed on the surface of the borophene sheets.

HER performance of borophene was assessed by electrochemical measurements including LSV, CV and EIS. Equal amount of carbon black was added to the catalysts to provide good electrical conductivity. Figure 4a shows the SEM image of the borophene electrode used in the HER measurements. Borophene sheets and carbon black nanoparticles form a homogeneous mixture ensuring good electrode conductivity. The electrode has a porous structure which facilitates all active sites to be accessible. Some individual borophene sheets seem to be well dispersed in the carbon black matrix while the others form

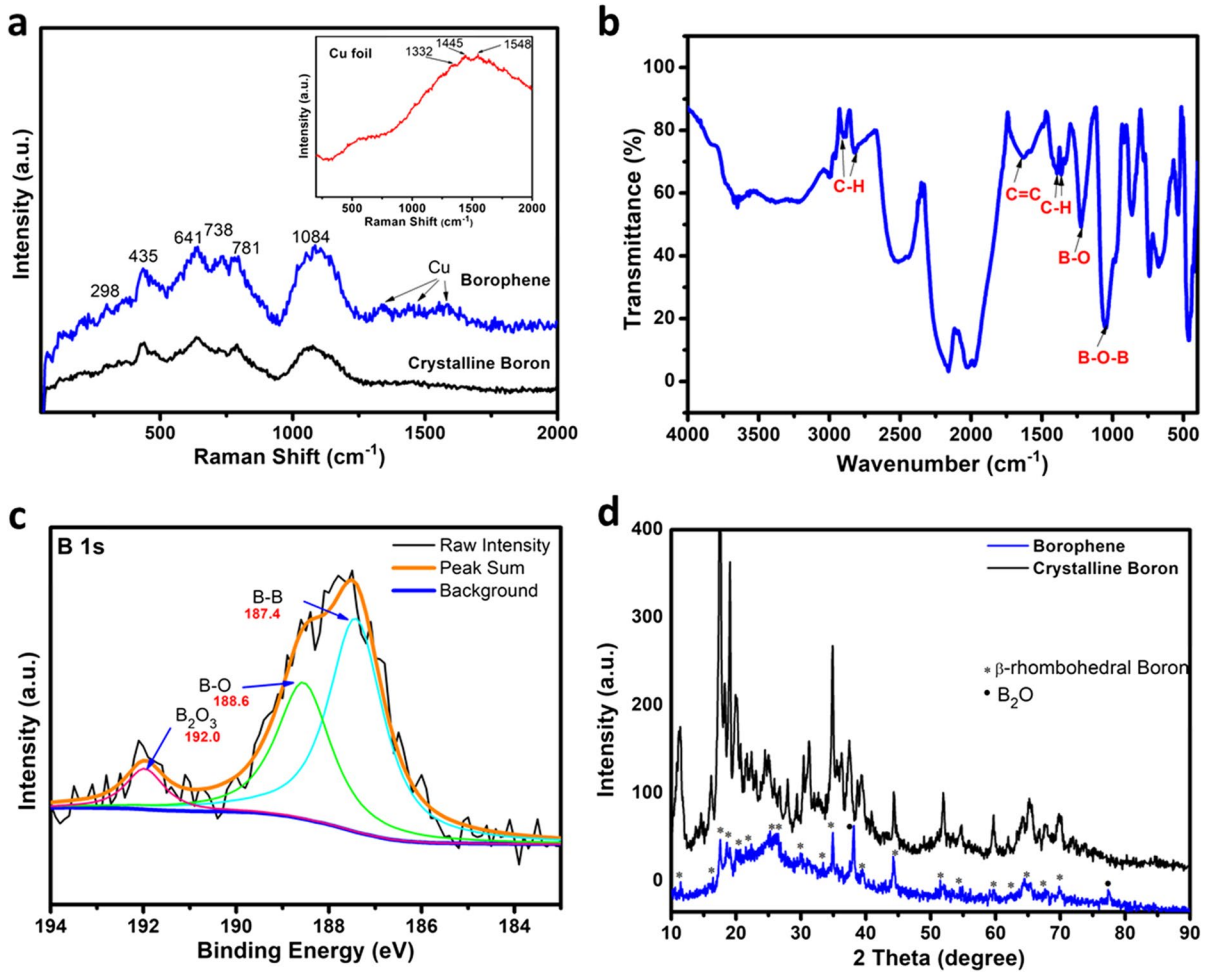

Fig. 3 (**a**) Raman spectra of crystalline boron powder and borophene sheets drop casted on a piece of Cu foil (Inset shows the Raman spectra of bare Cu foil). (**b**) FTIR and (**c**) XPS B 1 s spectra of borophene. (**d**) XRD patterns of the crystalline boron powder and borophene sheets

agglomerates. Such agglomerates are undesirable because they decrease the total electrochemical surface area (ECSA). The EDX spectrum taken from the sample indicates the presence of B, C and O elements (Fig. 4b). The elemental ratio of B/O was found to be 95%, which indicates that only the surface of the borophene sheets is oxidized. Figure 5a shows the polarization curves of superP, bulk boron, uncentrifuged borophene and centrifuged borophene among which the centrifuged borophene is the most active catalyst as indicated by its lowest overpotential and largest current density. The overpotential of the centrifuged borophene to drive a current density of 10 mA cm^{-2} is 480 mV, which is 58 and 152 mV lower than that of the uncentrifuged borophene and bulk boron powder, respectively. On the other hand, superP shows only a negligible activity over the potential range of the measurements. Tafel analysis was performed to evaluate the reaction kinetics of the catalysts and elucidate the reaction mechanism. Tafel slopes were deduced by fitting the Tafel plots (Fig. 5b) to Tafel equation [53], $\eta = blogj + a$, where η is the overpotential and b is the Tafel slope. The smaller Tafel slope values indicate faster reaction kinetics [54]. The HER kinetics of bulk boron was improved after the exfoliation as evident by the significantly smaller Tafel slopes

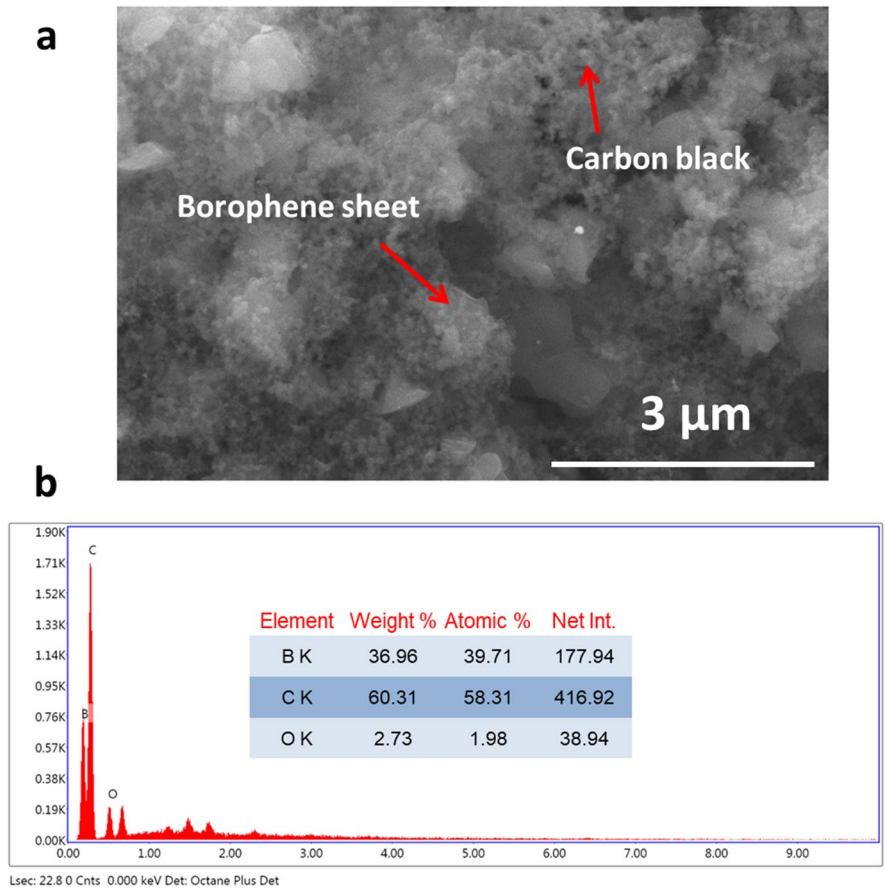

Fig. 4 (**a**) SEM image of a borophene electrode used in the HER measurements. (**b**) EDX spectrum taken from the electrode surface and the corresponding elemental ratios

of the borophene samples. The centrifuged (163 mV dec^{-1}) and uncentrifuged borophene (152 mV dec^{-1}) samples have similar Tafel slope values. As the uncentrifuged borophene sample contains relatively thicker and larger sheets, we can infer that the effect of thickness and lateral size of the borophene sheets on the HER kinetics is insignificant. The Tafel slope values of the borophene samples over 120 mV dec^{-1} suggest Volmer-Heyrovsky reaction mechanism with a rate limiting step of proton adsorption [55]. EIS measurements were conducted at an overpotential of 480 mV to investigate the charge transfer kinetics of the catalysts. The resulting Nyquist plots (Fig. 5c) exhibit incomplete semicircle, which could be due to inhomogeneous electrode surface [56]. Nyquist plots could be well fitted to a modified Randle's model (Fig. 5c inset), which gave the charge transfer resistance (R_{ct}) values of 1717, 1572 and 834 Ω for the bulk boron, uncentrifuged borophene and centrifuged borophene, respectively. The lowest R_{ct} of the centrifuged borophene implies a superior charge transfer rate at the electrode/electrolyte interface compared to others. The stability of the best performing catalyst was assessed by monitoring the current density at a constant potential. The starting current density was 10 mA cm^{-2}, which slowly dropped to 8.1 mA cm^{-2} after 16 h of operation, indicating 81% retention of its activity (Fig. 5d). The slight decrease of the catalytic activity may be due to the clinging H_2 bubbles that block the active sites.

To further clarify the enhanced HER activity of the exfoliated borophene, C_{dl} values were extracted from the slopes of the Δj–scan rate plots (Fig. 6a), which gave 1810, 1115 and 870 µF cm^{-2} for the centrifuged borophene, uncentrifuged borophene and bulk boron, respectively. As the ECSA is proportional to C_{dl} [57], the ECSA of the centrifuged borophene is 1.7 times larger than the uncentrifuged borophene and 2.8 times

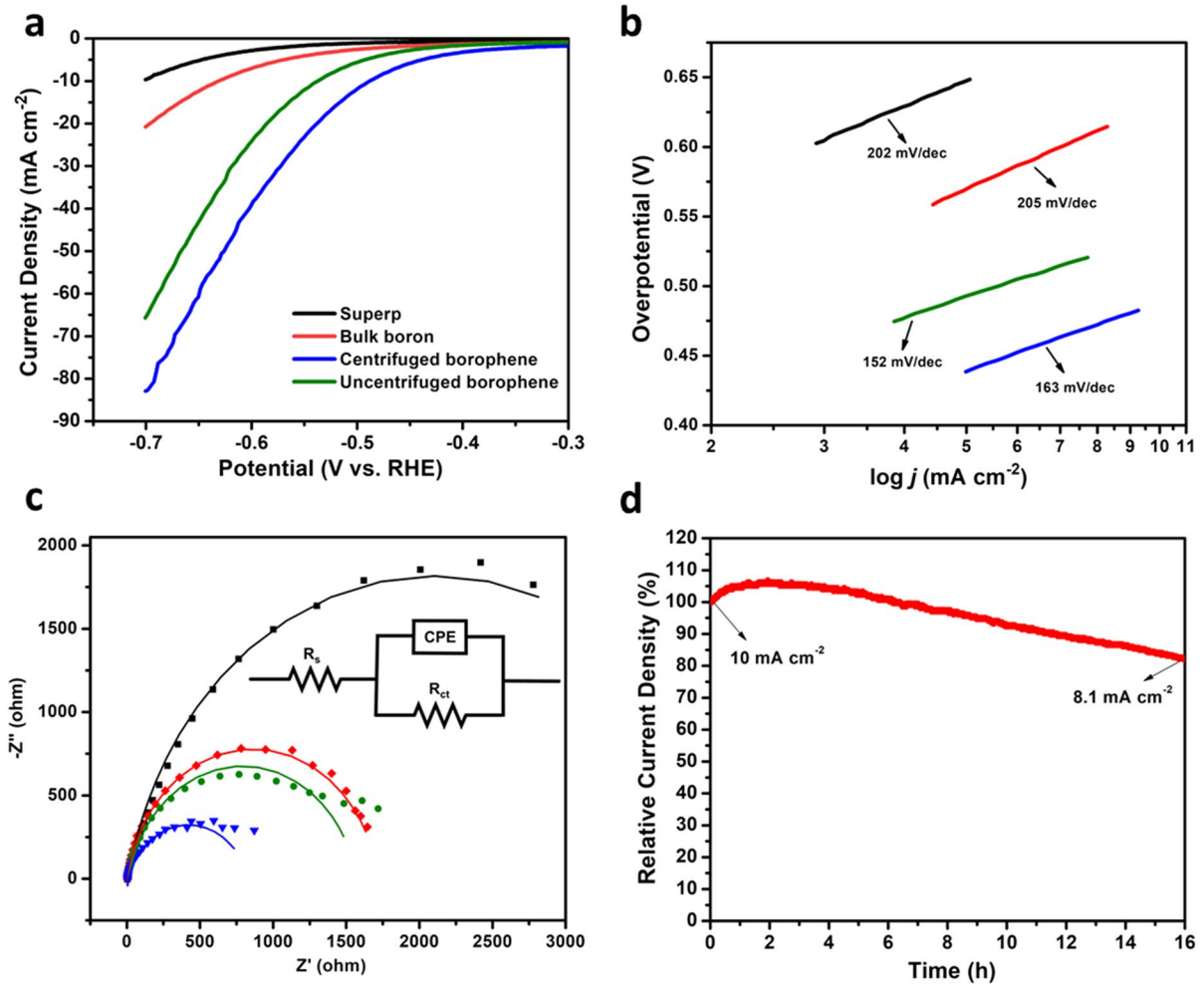

Fig. 5 (**a**) LSV curves, (**b**) Tafel plots and (**c**) Nyquist plots of superP, bulk boron, uncentrifuged and centrifuged borophene. (**d**) Stability test of the centrifuged borophene over a period of 16 h

larger than the bulk boron. The polarization curves were normalized by the ECSA in order to exclude the effect of surface area on the HER performance of the catalysts and compare the intrinsic activity of the samples. The normalized polarization curves are displayed in Fig. 6b, in which the centrifuged and uncentrifuged borophene exhibit similar HER activity whereas the overpotential of the bulk boron is 65 mV larger. This implies that when the bulk boron is exfoliated to borophene sheets not only the surface area is increased but also the intrinsic activity is improved, leading to an overall 152 mV reduction in the overpotential. Moreover, the superior HER performance of the centrifuged borophene compared to uncentrifuged one can be solely attributed to its larger ECSA.

The oxidized surface of borophene should also have an effect on the HER activity. The effect of the surface oxidation on the HER activity of borophene sheets can be discussed by taking consideration of oxidized Pt. Recently, Yu et al. reported that oxidized Pt exhibits better electrocatalytic activity in HER compared to metallic Pt, which was attributed to accelerated coupling of electrons and protons on Pt-O sites, leading to faster H_2 release [58]. Furthermore, Cheng et al. demonstrated that oxidized Pt clusters are more active in HER compared to commercial Pt/C

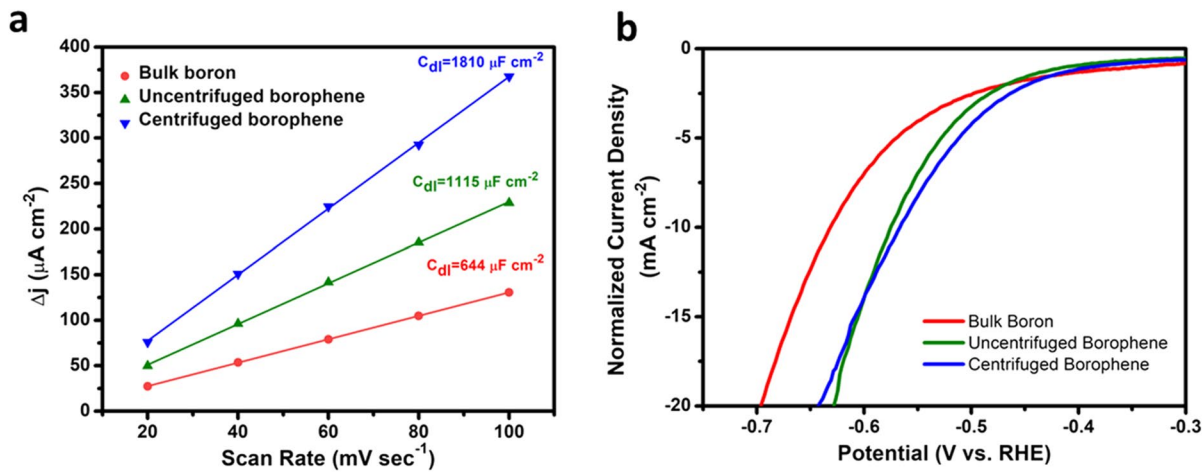

Fig. 6 (**a**) Δj–scan rate plots and (**b**) normalized polarization curves of the bulk boron, uncentrifuged and centrifuged borophene samples

catalyst [59]. Similarly, the B-O bonds on the borophene surface may be favorable for HER. Such oxidized surface is also beneficial for the chemical stability of borophene in acidic media.

The HER performance of the electrochemically exfoliated borophene was compared with other borophene catalysts and some electrochemically exfoliated TMD materials in Table 1. The electrochemically exfoliated borophene performs better than the surfactant-assisted exfoliated borophene with a lower overpotential and Tafel slope values. However, the HER performance of the electrochemically exfoliated borophene is low compared to CVD grown borophene on carbon cloth and electrochemically exfoliated TMD nanosheets.

Conclusion

In conclusion, we have demonstrated catalytic activity of electrochemically exfoliated borophene in HER. Few layer borophene sheets with an average thickness of 8.3 nm were produced by anodic exfoliation of crystalline boron particles in Na_2SO_4. The exfoliated borophene sheets are high crystalline with a β-rhombohedral crystal structure and exhibit an oxidized surface mainly composed of boron-suboxides. Borophene shows enhanced catalytic activity in HER compared to bulk boron accompanied with decent stability. Electrochemical measurements revealed that faster HER kinetics as indicated by the smaller Tafel slope and the

Table 1 Comparison of HER performance of the electrochemically exfoliated borophene with other borophene catalysts and some electrochemically exfoliated TMD materials reported in literature

Material	Overpotential at 10 mA cm^{-2}	Tafel Slope	Reference
CVD grown borophene on carbon cloth	142 mV	69 mV dec^{-1}	[34]
Surfactant-assisted exfoliated borophene sheets	645 mV	173 mV dec^{-1}	[35]
Electrochemically exfoliated TaS_2 nanosheets	197 mV	100 mV dec^{-1}	[60]
Electrochemically exfoliated NbS_2 nanosheets	90 mV	83 mV dec^{-1}	[61]
Electrochemically exfoliated MoS_2 nanosheets	500 mV	74 mV dec^{-1}	[62]
Electrochemically exfoliated borophene sheets	480 mV	163 mV dec^{-1}	This work

larger ESCA are responsible for the enhanced catalytic activity of borophene. The ECSA normalized polarization curves of the centrifuged and uncentrifuged borophene almost overlap, indicating that size and thickness have negligible effect on the intrinsic activity of borophene.

Acknowledgements We would like to thank The Scientific and Technological Research Council of Turkey for their financial support.

Author contribution C.K. and D.K. conceptualized the idea. C.K. supervised the work and interpreted the obtained data. D.K. received the funding. S.C. conducted the experiments and prepared the figues. All authors contributed to the preparation of the manuscript.

Funding This work was funded by The Scientific and Technological Research Council of Turkey (Grand No. 222M300).

Data availability statement The data that support the findings of this study are available from the corresponding author upon reasonable request. No datasets were generated or analysed during the current study.

Declarations

Conflict of Interests The authors declare no competing interests.

References

1. Soeder DJ (2021) Fracking and the Environment: A scientific assessment of the environmental risks from hydraulic fracturing and fossil fuels. Springer
2. Wuebbles DJ, Jain AK (2001) Concerns about climate change and the role of fossil fuel use. Fuel Process Technol 71(1–3):99–119. https://doi.org/10.1016/S0378-3820(01)00139-4
3. Johnsson F, Kjärstad J, Rootzén J (2019) The threat to climate change mitigation posed by the abundance of fossil fuels. Clim Policy 19(2):258–274. https://doi.org/10.1080/14693062.2018.1483885
4. Seinfeld JH (2011) Insights on global warming. AIChE J 57(12):3259–3284. https://doi.org/10.1002/aic.12780
5. Tanaka K, O'Neill BC (2018) The Paris Agreement zero-emissions goal is not always consistent with the 1.5 C and 2 C temperature targets. Nat Clim Change 8(4):319–324. https://doi.org/10.1038/s41558-018-0097-x
6. Müller K, Arlt W (2013) Status and development in hydrogen transport and storage for energy applications. Energy Technol 1(9):501–511. https://doi.org/10.1002/ente.201300055
7. Kalamaras CM, Efstathiou AM (2013) Hydrogen production technologies: current state and future developments. In Conference Papers in Science Hindawi
8. Patonia A, Poudineh R (2022) Cost-competitive green hydrogen: how to lower the cost of electrolysers?. Oxford Institute for Energy Studies
9. Nguyen MTD, Ranjbari A, Catala L, Brisset F, Millet P, Aukauloo A (2012) Implementing molecular catalysts for hydrogen production in proton exchange membrane water electrolysers. Coord Chem Rev 256(21–22):2435–2444. https://doi.org/10.1016/j.ccr.2012.04.040
10. Scott K (2019) Electrochemical Methods for Hydrogen Production. RSC
11. Lagadec MF, Grimaud A (2020) Water electrolysers with closed and open electrochemical systems. Nat Mater 19(11):1140–1150. https://doi.org/10.1038/s41563-020-0788-3
12 Das S, Kim M, Lee JW, Choi W (2014) Synthesis, properties, and applications of 2-D materials: A comprehensive review. Crit Rev Solid State Mater Sci 39(4):231–252. https://doi.org/10.1080/10408436.2013.83.6075
13. Gupta A, Sakthivel T, Seal S (2015) Recent development in 2D materials beyond graphene. Prog Mater Sci 73:44–126. https://doi.org/10.1016/j.pmatsci.2015.02.002
14 Glavin NR, Rao R, Varshney V, Bianco E, Apte A, Roy A, Ringe E, Ajayan PM (2020) Emerging applications of elemental 2D materials. Adv Mater 32(7):1904302. https://doi.org/10.1002/adma.201904302
15. Butler SZ, Hollen SM, Cao L, Cui Y, Gupta JA, Gutiérrez HR, Heinz TF, Hong SS, Huang J, Ismach AF, Johnston-Halperin E (2013) Progress, challenges, and opportunities in two-dimensional materials beyond graphene. ACS Nano 7(4):2898–2926. https://doi.org/10.1021/nn400280c
16. Voiry D, Yang J, Chhowalla M (2016) Recent strategies for improving the catalytic activity of 2D TMD nanosheets toward the hydrogen evolution reaction. Adv Mater 28(29):6197–6206. https://doi.org/10.1002/adma.201505597
17. Mondal A, Vomiero A (2022) 2D transition metal dichalcogenides-based electrocatalysts for hydrogen evolution reaction. Adv Funct Mater 32(52):2208994. https://doi.org/10.1002/adfm.202208994
18 Wang Z, Tang MT, Cao A, Chan K, Nørskov JK (2022) Insights into the hydrogen evolution reaction on 2D transition-metal dichalcogenides. J Phys Chem C 126(11):5151–5158. https://doi.org/10.1021/acs.jpcc.1c10436
19. Bai S, Yang M, Jiang J, He X, Zou J, Xiong Z, Liao G, Liu S (2021) Recent advances of MXenes as electrocatalysts for hydrogen evolution reaction. npj 2D Mater Appl 5(1):78. https://doi.org/10.1038/s41699-021-
20. Gao G, O'Mullane AP, Du A (2017) 2D MXenes: a new family of promising catalysts for the hydrogen evolution reaction. ACS Catal 7(1):494–500. https://doi.org/10.1021/acscatal.6b02754
21. Glavin NR, Rao R, Varshney V, Bianco E, Apte A, Roy A, Ringe E, Ajayan PM (2020) Emerging applications of elemental 2D materials. Adv Mater 32(7):1904302. https://doi.org/10.1002/adma.201904302
22. Mannix AJ, Kiraly B, Hersam MC, Guisinger NP (2017) Synthesis and chemistry of elemental 2D materials. Nat Rev Chem 1(2):0014. https://doi.org/10.1038/s41570-016-0014

23. Fan FR, Wang R, Zhang H, Wu W (2021) Emerging beyond-graphene elemental 2D materials for energy and catalysis applications. Chem Soc Rev 50(19):10983–11031 https://doi.org/10.1039/C9CS00821G
24. Ranjan P, Lee JM, Kumar P, Vinu A (2020) Borophene: New sensation in flatland. Adv Mater 32(34):2000531. https://doi.org/10.1002/adma.202000531
25. Ou M, Wang X, Yu L, Liu C, Tao W, Ji X, Mei L (2021) The emergence and evolution of borophene. Adv Sci 8(12):2001801. https://doi.org/10.1002/advs.202001801
26. Hou C, Tai G, Wu Z, Hao J (2020) Borophene: current status, challenges and opportunities. ChemPlusChem 85(9):2186–2196. https://doi.org/10.1002/cplu.202000550
27. Mannix AJ, Zhang Z, Guisinger NP, Yakobson BI, Hersam MC (2018) Borophene as a prototype for synthetic 2D materials development. Nat Nanotechnol 13(6):444–450. https://doi.org/10.1038/s41565-018-0157-4
28. Yu E, Pan Y (2022) Exploring the hydrogen evolution catalytic activity of the orthorhombic and hexagonal borophene as the hydrogen storage material. Electrochim Acta 435:141391. https://doi.org/10.1016/j.electacta.2022.141391
29. Xing N, Gao N, Ye P, Yang X, Wang H, Zhao J (2024) Bilayer borophene: an efficient catalyst for hydrogen evolution reaction. Front Chem Sci Eng 18(3):26. https://doi.org/10.1007/s11705-024-2389-1
30. Rubab A, Baig N, Sher M, Sohail M (2020) Advances in ultrathin borophene materials. J Chem Eng 401:126109. https://doi.org/10.1016/j.cej.2020.126109
31. Lin Y, Yu M, Li X, Gao W, Wang L, Zhao X, Zhou M, Yao X, He M, Zhang X (2021) Designed borophene/TMDs hybrid catalysts for enhanced hydrogen evolution reactions. J Mater Chem C 9(44):15877–15885. https://doi.org/10.1039/D1TC04197E
32. Yu E, Pan Y (2024) Enhancing the catalytic hydrogen evolution reaction (HER) of the defective borophene@Pt/Pd/MoS_2 heterojunction. Int J Hydrogen Energy 50:920–931. https://doi.org/10.1016/j.ijhydene.2023.08.238
33. Yu E, Pan Y (2022) Catalytic properties of borophene/MoS_2 heterojunctions for hydrogen evolution reaction under different stacking conditions. J Mater Chem A 10(46):24866–24876. https://doi.org/10.1039/D2TA05928B
34. Tai G, Xu M, Hou C, Liu R, Liang X, Wu Z (2021) Borophene nanosheets as high-efficiency catalysts for the hydrogen evolution reaction. ACS Appl Mater Interfaces 13(51):60987–60994. https://doi.org/10.1021/acsami.1c15953
35. Radhakrishnan S, Padmanabhan NT, Mathews AJ, Tang Y, Santhanakrishnan T, John H (2024) Surfactant-Assisted Restructuring of Boron to Borophene: Implications for Enhanced Hydrogen Evolution. ACS Appl Nano Mater 7(11):12564–12578. https://doi.org/10.1021/acsanm.4c01017
36. Kiraly B, Liu X, Wang L, Zhang Z, Mannix AJ, Fisher BL, Yakobson BI, Hersam MC, Guisinger NP (2019) Borophene synthesis on Au (111). ACS Nano 13(4):3816–3822. https://doi.org/10.1021/acsnano.8b09339
37. Zhong Q, Kong L, Gou J, Li W, Sheng S, Yang S, Cheng P, Li H, Wu K, Chen L (2017) Synthesis of borophene nanoribbons on Ag (110) surface. Phys Rev Mater 1(2):021001. https://doi.org/10.1103/PhysRevMaterials.1.021001
38. Sutter P, Sutter E (2021) Large-scale layer-by-layer synthesis of borophene on Ru (0001). Chem Mater 33(22):8838–8843. https://doi.org/10.1021/acs.chemmater.1c03061
39. Zhang F, She L, Jia C, He X, Li Q, Sun J, Lei Z, Liu ZH (2020) Few-layer and large flake size borophene: preparation with solvothermal-assisted liquid phase exfoliation. RSC Adv 10(46):27532–27537. https://doi.org/10.1039/d0ra03492d
40. Ranjan P, Sahu TK, Bhushan R, Yamijala SS, Late DJ, Kumar P, Vinu A (2019) Freestanding borophene and its hybrids. Adv Mater 31(27):1900353. https://doi.org/10.1002/adma.201900353
41. Lin H, Shi H, Wang Z, Mu Y, Li S, Zhao J, Guo J, Yang B, Wu ZS, Liu F (2021) Scalable production of free-standing Few-layer β12-borophene single crystalline sheets as efficient electrocatalysts for lithium–sulfur batteries. ACS Nano 15(11):17327–17336. https://doi.org/10.1021/acsnano.1c04961
42. Li H, Jing L, Liu W, Lin J, Tay RY, Tsang SH, Teo EHT (2018) Scalable production of few-layer boron sheets by liquid-phase exfoliation and their superior supercapacitive performance. ACS Nano 12(2):1262–1272. https://doi.org/10.1021/acsnano.7b07444
43. Kuru D, Kuru C (2024) A new route to electrochemical exfoliation of borophene for scalable production. J Mater Sci. https://doi.org/10.1007/s10853-024-09769-0
44. Zielinkiewicz K, Baranowska D, Mijowska E (2023) Ball milling induced borophene flakes fabrication. RSC Adv 13(25):16907–16914. https://doi.org/10.1039/D3RA02400H
45. Parakhonskiy G, Dubrovinskaia N, Bykova E, Wirth R, Dubrovinsky L (2011) Experimental pressure-temperature phase diagram of boron: resolving the long-standing enigma. Sci Rep 1(1):96. https://doi.org/10.1038/srep00096
46. Sheng S, Wu JB, Cong X, Zhong Q, Li W, Hu W, Gou J, Cheng P, Tan PH, Chen L, Wu K (2019) Raman spectroscopy of two-dimensional borophene sheets. ACS Nano 13(4):4133–4139. https://doi.org/10.1021/acsnano.8b08909
47. Abdi Y, Mazaheri A, Hajibaba S, Darbari S, Rezvani SJ, Cicco AD, Paparoni F, Rahighi R, Gholipour S, Rashidi A, Byranvand MM (2022) A two-dimensional borophene supercapacitor. ACS Mater Lett 4(10):1929–1936. https://doi.org/10.1021/acsmaterialslett.2c00475
48. Rivera-Tello CD, Guerrero JA, Huerta L, Flores-Ruiz FJ, Flores M, Quiñones-Galván JG (2023) Influence of plasma kinetic energy during the pulsed laser deposition of borophene films on silicon (100). RSC Adv 13(43):29819–29829. https://doi.org/10.1039/D3RA04601J
49. Taşaltın N, Güllülü S, Karakuş S (2022) Dual-role of β borophene nanosheets as highly effective antibacterial and antifungal agent. Inorg Chem Commun 136:109150. 1016/j.inoche.2021.109150
50. Yao C, Xie A, Shen Y, Zhu J, Li T (2013) Green synthesis of calcium carbonate with unusual morphologies in the presence of fruit extracts. J Chil Chem Soc 58(4):2235–2238. https://doi.org/10.4067/S0717-97072013000400072
51. Fu P, Hu S, Xiang J, Li P, Huang D, Jiang L, Zhang A, Zhang J (2010) FTIR study of pyrolysis products evolving

from typical agricultural residues. J Anal Appl Pyrol 88(2):117–123. https://doi.org/10.1016/j.jaap.2010.03.004
52. Rohani P, Kim S, Swihart MT (2016) Boron nanoparticles for room-temperature hydrogen generation from water. Adv Energy Mater 6(12):1502550. https://doi.org/10.1002/aenm.201502550
53. Petrii OA, Nazmutdinov RR, Bronshtein MD, Tsirlina GA (2007) Life of the Tafel equation: Current understanding and prospects for the second century. Electrochim Acta 52(11):3493–3504. https://doi.org/10.1016/j.electacta.2006.10.014
54. Wang JX, Uribe FA, Springer TE, Zhang J, Adzic RR (2009) Intrinsic kinetic equation for oxygen reduction reaction in acidic media: the double Tafel slope and fuel cell applications. Farad Disc 140:347–362. https://doi.org/10.1039/B802218F
55. Li Y, Wang H, Xie L, Liang Y, Hong G, Dai H (2011) MoS_2 nanoparticles grown on graphene: an advanced catalyst for the hydrogen evolution reaction. J Am Chem Soc 133(19):7296–7299. https://doi.org/10.1021/ja201269b
56. Cheng Q, Chen Z (2013) The cause analysis of the incomplete semi-circle observed in high frequency region of EIS obtained from TEL-covered pure copper. Int J Electrochem Sci 8(6):8282–8290. https://doi.org/10.1016/S1452-3981(23)12887-2
57. Ren H, Pan Y, Sorrell CC, Du H (2020) Assessment of electrocatalytic activity through the lens of three surface area normalization techniques. J Mater Chem A 8(6):3154–3159. https://doi.org/10.1039/C9TA13170A
58. Yu FY, Lang ZL, Yin Y, Feng K, Xia YJ, Tan HQ, Zhu HT, Zhong J, Kang ZH, Li YG (2020) Pt-O bond as an active site superior to Pt0 in hydrogen evolution reaction. Nat Commun 11(1):490. https://doi.org/10.1038/s41467-019-14274-z
59. Cheng X, Li Y, Zheng., Yan Y, Zhang Y, Chen G, Sun S, Zhang J, (2017) Highly active, stable oxidized platinum clusters as electrocatalysts for the hydrogen evolution reaction. Energy Environ Sci 10(11):2450–2458. https://doi.org/10.1039/C7EE02537H
60. Chen H, Si J, Lyu S, Zhang T, Li Z, Lei C, Lei L, Yuan C, Yang B, Gao L, Hou Y (2020) Highly effective electrochemical exfoliation of ultrathin tantalum disulfide nanosheets for energy-efficient hydrogen evolution electrocatalysis. ACS Appl Mater Interfaces 12(22):24675–24682. https://doi.org/10.1021/acsami.9b15039
61. Si J, Zheng Q, Chen H, Lei C, Suo Y, Yang B, Zhang Z, Li Z, Lei L, Hou Y, Ostrikov K (2019) Scalable production of few-layer niobium disulfide nanosheets via electrochemical exfoliation for energy-efficient hydrogen evolution reaction. ACS Appl Mater Interfaces 11(14):13205–13213. https://doi.org/10.1021/acsami.8b22052
62. Ambrosi A, Pumera M (2018) Electrochemical exfoliation of MoS2 crystal for hydrogen electrogeneration. Chem A Eur J 24(69):18551–18555. https://doi.org/10.1002/chem.201804821